Towards Real-time Radio-SLAM via Optimal Importance Sampling

Citation for the original published paper (version of record):
Kaltiokallio, O., Hostettler, R., Talvitie, J. et al (2022). Towards Real-time Radio-SLAM via Optimal Importance Sampling. IEEE Workshop on Signal Processing Advances in Wireless Communications, SPAWC, 2022-July. http://dx.doi.org/10.1109/SPAWC51304.2022.9833982

Towards Real-time Radio-SLAM via Optimal Importance Sampling

Ossi Kaltiokallio[†], Roland Hostettler[‡], Jukka Talvitie[†], Yu Ge[⋆],
Hyowon Kim[⋆], Henk Wymeersch[⋆], and Mikko Valkama[†]

[†]Unit of Electrical Engineering, Tampere University, Tampere, Finland
[‡]Department of Electrical Engineering, Uppsala University, Uppsala, Sweden
[⋆]Department of Electrical Engineering, Chalmers University of Technology, Göteborg, Sweden

***Abstract*—In future cellular networks, it will be possible to estimate the channel parameters of non-line-of-sight propagation paths providing unique opportunities for simultaneous localization and mapping (SLAM) with commodity user equipments (UEs). Radio-SLAM generally relies on generating samples of the UE trajectory and constructing a trajectory-conditioned map. To reduce the number of samples and complexity, we propose an iterative method to approximate the optimal sampling density. The numerical results demonstrate that the added computational complexity of the proposed method can be easily justified by the more efficient use of particles. As an outcome, the presented filter nearly achieves the lower bound and still runs in real-time.**

***Index Terms*—millimeter wave, simultaneous localization and mapping, probability hypothesis density, importance density**

I. Introduction

The high temporal and spatial resolution of the fifth generation (5G) millimeter wave (mmWave) and the future sixth generation (6G) systems provide unique opportunities in positioning and sensing [1]. Downlink mmWave positioning reference signals (PRS) can be sent from the base station (BS) to the user equipment (UE) along the line-of-sight (LOS) and/or non-line-of-sight (NLOS) paths. At the UE side, the PRS are received and state-of-the-art channel estimators [2] can provide channel gain, time of arrival (TOA), angle of arrival (AOA) and angle of departure (AOD) estimates for the propagation paths. The intrinsic connection of the NLOS paths to the propagation environment together with the channel estimates enables not only localization but also mapping the environment [3].

The process of jointly localizing the UE and creating a map of the environment is known as simultaneous localization and mapping (SLAM), often referred to as Radio-SLAM in the mmWave context. Several different solutions to the problem exist including: geometry-based methods [4], belief propagation algorithms [5] and methods relying on random finite set (RFS) theory [6]. Formulating the Radio-SLAM problem using RFSs has proven to be a noteworthy candidate [6]–[10], and the attractiveness of the method lies in the fact that it enables a fully integrated Bayesian framework for Radio-SLAM. The RFS methods can inherently deal with the challenges of Radio-SLAM and these are: data association uncertainty, unknown number of map features, clutter measurements and misdetections [6]. One approach to solve the problem is based on an exact factorization of the posterior into a product of conditional landmark distributions and a distribution over UE trajectories [11]. The nonlinear UE trajectory is targeted using a particle filter (PF) and the trajectory-conditioned map is estimated with a probability hypothesis density (PHD) [6] or a Poisson multi-Bernoulli mixture [7] filter. The aforementioned works typically require a large number of particles, severely impacting the computational overhead. A better choice of the importance density allows for fewer particles without loss of performance, as was shown in FastSLAM 2.0 which used an optimal importance density (OID) approximation [12].

In this paper, a better approximation of the importance density is presented so that the UE posterior can be represented with fewer particles. We exploit an iterative method for approximating the OID, which is based on using generalized statistical linear regression (SLR), combined with iterated posterior linearization (IPL) [13], [14]. In Radio-SLAM, the use of SLR and IPL was first demonstrated in [10], and it was shown that the approach has certain benefits. It is worth noting that in this paper IPL is used to approximate the OID, whereas in [10], IPL is used to update the joint posterior SLAM density.

To the best of our knowledge, this is the first time a joint OID approximation is applied to RFS-SLAM. Moreover, the proposed method overcomes two important limitations of the one-step OID approximation used in FastSLAM 2.0. First of all, the one-step OID approximation may not work for certain types of non-Gaussian likelihoods. Second, linearization is conducted around the prior, not the posterior.

II. RFS-Based SLAM

A. Radio-SLAM Models

This paper focuses on a feature-based approach that decomposes the physical environment into parametric point representation referred to as landmarks. As illustrated in Fig.1, we consider three types of landmarks: (i) BS for which the location is known; (ii) reflecting surfaces modeled as virtual anchors (VAs) and; (iii) small objects that are modeled as

This work was partially supported by the Academy of Finland under grants #328214, #323244, #319994, and #338224, by the Wallenberg AI, Autonomous Systems and Software Program (WASP) funded by Knut and Alice Wallenberg Foundation, and the Vinnova 5GPOS project under grant 2019-03085.

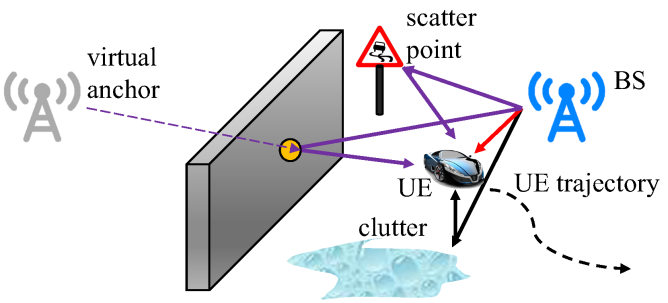

Fig. 1. In Radio-SLAM, a UE simultaneously localizes itself and builds a map of the environment using channel parameter estimates.

scattering points (SPs) [6]. The state of the landmarks is $\mathbf{m} = [\mathbf{m}_{\mathrm{LM}}^{\mathsf{T}},\ m_{\mathrm{ST}}]^{\mathsf{T}}$, where $\mathbf{m}_{\mathrm{LM}} \in \mathbb{R}^3$ is the 3D location and $m_{\mathrm{ST}} \in \{\mathrm{BS}, \mathrm{VA}, \mathrm{SP}\}$ the source type. The UE state is given by $\mathbf{s} = [x,\ y,\ \alpha,\ B]^{\mathsf{T}}$, where $[x,\ y]^{\mathsf{T}}$ is the 2D location, α the vehicle heading and B the bias between the UE and network clocks. For further details, the reader is referred to [6], [8]–[10].

The underlying state-space model is represented by

$$\mathbf{s}_k \sim p(\mathbf{s}_k|\mathbf{s}_{k-1}, \mathbf{u}_k), \tag{1a}$$

$$\mathbf{z}_k^n \sim p(\mathbf{z}_k|\mathbf{s}_k, \mathbf{m}^j), \tag{1b}$$

where k denotes the time and $\mathbf{u}_k = [\nu_k,\ \omega_k]^{\mathsf{T}}$ is a deterministic speed ν_k and angular velocity ω_k control command of the UE. The n-th measurement is denoted as $\mathbf{z}_k^n$, and it contains the TOA (depending on $[x_k,\ y_k]^{\mathsf{T}}$ and B_k), AOA (depending on $[x_k,\ y_k]^{\mathsf{T}}$ and α_k) and AOD (depending on $[x_k,\ y_k]^{\mathsf{T}}$) estimates, and the intrinsic connection of the channel parameters to the BS, landmark and UE pose is presented [6]. Since the number of landmarks in the field-of-view (FOV) is unknown, the map and measurements are represented with finite sets, $\mathcal{M}_k = \{\mathbf{m}^1, \mathbf{m}^2, \ldots, \mathbf{m}^{|\mathcal{M}_k|}\}$ and $\mathcal{Z}_k = \{\mathbf{z}^1, \mathbf{z}^2, \ldots, \mathbf{z}^{|\mathcal{Z}_k|}\}$ respectively, and $|\cdots|$ denotes the cardinality of a set. Due to imperfections in the receiver and channel estimator, it is also possible that $\mathbf{m}^j \in \mathcal{M}_k$ is not detected and $\mathbf{z}_k^n \in \mathcal{Z}_k$ corresponds to clutter.

B. PHD-SLAM Filter

In probabilistic form, the SLAM problem aims to estimate the joint posterior density of the landmarks and UE trajectory, given the initial state $\mathbf{s}_0$, recorded observations $\mathcal{Z}_{1:k}$ and control inputs $\mathbf{u}_{1:k}$ up to and including time k. The joint posterior RFS-SLAM density can be decomposed as [11]

$$\begin{aligned} &p(\mathbf{s}_{1:k}, \mathcal{M}_k|\mathcal{Z}_{1:k}, \mathbf{u}_{1:k}, \mathbf{s}_0) \\ &\qquad = p(\mathbf{s}_{1:k}|\mathcal{Z}_{1:k}, \mathbf{u}_{1:k}, \mathbf{s}_0) p(\mathcal{M}_k|\mathcal{Z}_{1:k}, \mathbf{s}_{0:k}). \end{aligned} \tag{2}$$

Now, the nonlinear UE trajectory $\mathbf{s}_{0:k}$ can be tracked using a PF and the trajectory-conditioned map is estimated using a PHD. The overall PHD-SLAM density at time k is represented by a set of N particles, $\left\{w_k^{(i)}, \mathbf{s}_{0:k}^{(i)}, v_k^{(i)}(\mathbf{m}|\mathbf{s}_k^{(i)})\right\}_{i=1}^{N}$, where $w_k^{(i)}$, $\mathbf{s}_{0:k}^{(i)}$ and $v_k^{(i)}(\mathbf{m}|\mathbf{s}_k^{(i)})$ are the weight, trajectory and PHD of particle i, respectively. The PHD is parametrized using a Gaussian mixture (GM) [15]

$$v_{k|k}^{(i)}(\mathbf{m}|\mathbf{s}_k^{(i)}) = \sum_{j=1}^{J_{k|k}^{(i)}} \eta_{k|k}^{(i,j)} \mathcal{N}(\boldsymbol{\mu}_{k|k}^{(i,j)}, \boldsymbol{\Sigma}_{k|k}^{(i,j)}), \tag{3}$$

where $J_{k|k}^{(i)}$ is the number of GM components at time k and, $\eta_{k|k}^{(i,j)}$, $\mu_{k|k}^{(i,j)}$ and $\Sigma_{k|k}^{(i,j)}$ are the weight, mean and covariance of landmark j for particle i in corresponding order.

1) PHD Mapping: Assume that the PHD at time $k-1$ is a GM of the form given in (3), then it follows that the predicted PHD at time k is also a GM given by [11]

$$v_{k|k-1}^{(i)}(\mathbf{m}|\mathbf{s}_k^{(i)}) = v_{k-1|k-1}^{(i)}(\mathbf{m}|\mathbf{s}_{k-1}^{(i)}) + v_{\mathrm{B},k}^{(i)}(\mathbf{m}|\mathbf{s}_k^{(i)}), \tag{4}$$

where the parameters of $v_{k-1|k-1}^{(i)}(\cdot)$ are unchanged since the landmarks are static, $v_{\mathrm{B},k}^{(i)}(\cdot)$ is the birth process with $J_{\mathrm{B},k}^{(i)}$ GM components, and the number of components in the predicted PHD is $J_{k|k-1}^{(i)} = J_{k-1|k-1}^{(i)} + J_{\mathrm{B},k}^{(i)}$. The birth process indicates where and with which intensities new landmarks appear. In this paper, the measurements are used to generate new landmarks as follows. First, a linearization point $\mathbf{m}_0$ is approximated using $\mathbf{z}_k^n$ and the inverse measurement function (see [6, Appendix D] and [9, Eq. (18)]). Second, the mean and Jacobian of the measurement model in (1b) are computed with respect to $\mathbf{m}_0$ and thereafter, location and covariance of the birth landmark are obtained by conditioning on $\mathbf{z}_k^n$. An uninformative prior with infinite covariance is utilized and the conditioning is computed in information form [16].

Given the measurement set $\mathcal{Z}_k$ at time k and the predicted PHD $v_{k|k-1}^{(i)}(\cdot)$, the posterior map PHD is a GM given by [11]

$$\begin{aligned} v_{k|k}^{(i)}(\mathbf{m}|\mathbf{s}_k^{(i)}) &= \left[1 - P_{\mathrm{D}}(\mathbf{m}|\mathbf{s}_k^{(i)})\right] v_{k|k-1}^{(i)}(\mathbf{m}|\mathbf{s}_k^{(i)}) \\ &\quad + \sum_{\mathbf{z}\in\mathcal{Z}_k} \frac{\boldsymbol{\Lambda}(\mathbf{m}|\mathbf{s}_k^{(i)})}{c(\mathbf{z}) + \int \boldsymbol{\Lambda}(\mathbf{m}'|\mathbf{s}_k^{(i)}) \mathrm{d}\mathbf{m}'}, \end{aligned} \tag{5}$$

where $P_{\mathrm{D}}(\mathbf{m}|\mathbf{s}_k^{(i)})$ is the adaptive detection probability [6], $c(\mathbf{z})$ is the PHD of the clutter RFS [15], and

$$\boldsymbol{\Lambda}(\mathbf{m}|\mathbf{s}_k^{(i)}) = P_{\mathrm{D}}(\mathbf{m}|\mathbf{s}_k^{(i)}) p(\mathbf{z}|\mathbf{s}_k^{(i)}, \mathbf{m}) v_{k|k-1}^{(i)}(\mathbf{m}|\mathbf{s}_k^{(i)}). \tag{6}$$

It is worth noting that every component of $v_{k|k-1}^{(i)}(\cdot)$ is updated by a miss detection and by every measurement such that the number of GM components in the updated PHD $v_{k|k}^{(i)}(\cdot)$ is $J_{k|k}^{(i)} = J_{k|k-1}^{(i)} \times (|\mathcal{Z}_k| + 1)$. This leads to an exponential growth in the number of GM components and therefore, the GM pruning algorithm proposed in [15] is used to reduce the number of GM components after each update.

2) UE Trajectory: The posterior of the UE trajectory, $p(\mathbf{s}_{1:k}|\mathcal{Z}_{1:k}, \mathbf{u}_{1:k}, \mathbf{s}_0)$, is estimated using the sequential importance resampling (SIR) PF [17] summarized in Algorithm 1. In the algorithm, the weight update requires solving $p(\mathcal{Z}_k|\mathcal{Z}_{1:k-1}, \mathbf{s}_{0:k}^{(i)})$. With a Poisson point process prior and a point object measurement model the solution is [6]

$$p(\mathcal{Z}_k|\mathcal{Z}_{1:k-1}, \mathbf{s}_{0:k}^{(i)}) = \prod_{\mathbf{z}\in\mathcal{Z}_k} c(\mathbf{z}) + \int \boldsymbol{\Lambda}(\mathbf{m}|\mathbf{s}_k^{(i)}) \mathrm{d}\mathbf{m}, \tag{7}$$

Algorithm 1 SIR particle filter

1: **for** $i = 1, \dots, N$ **do**
2: Compute importance density and sample from it

$$\mathbf{s}_k^{(i)} \sim q(\mathbf{s}_k | \mathbf{s}_{0:k-1}^{(i)}, \mathcal{Z}_{1:k}, \mathbf{u}_{1:k}) \tag{8}$$

3: Calculate the weights according to

$$w_k^{(i)} = w_{k-1}^{(i)} \frac{p(\mathcal{Z}_k | \mathcal{Z}_{1:k-1}, \mathbf{s}_{0:k}^{(i)}) p(\mathbf{s}_k^{(i)} | \mathbf{s}_{k-1}^{(i)}, \mathbf{u}_k)}{q(\mathbf{s}_k^{(i)} | \mathbf{s}_{0:k-1}^{(i)}, \mathcal{Z}_{1:k}, \mathbf{u}_{1:k})}. \tag{9}$$

4: **end for**
5: Normalize the weights $w_k^{(i)} = w_k^{(i)} / \sum_{i=1}^N w_k^{(i)}$ and compute the effective sample size $\text{ESS} = 1/\sum_{i=1}^N w_k^{(i)}$.
6: Resample if $\text{ESS} < N/2$

which can be evaluated during the PHD update step.

III. Importance Density

A. Data Association

To be able to compute the importance density, the data association between the measurements and landmarks must be solved first. The problem is casted as an optimal assignment problem as in [9] and solved using the auction algorithm [18]. After solving the optimal assignment, we introduce the concatenated state and measurement vectors

$$\mathbf{x}_k^{(i)} = \begin{bmatrix} (\mathbf{s}_k^{(i)})^\top & (\mathbf{m}^1)^\top & \dots (\mathbf{m}^M)^\top \end{bmatrix}^\top,$$
$$\mathbf{y}_k = \begin{bmatrix} (\mathbf{z}^{\ell(1)})^\top & \dots (\mathbf{z}^{\ell(M)})^\top \end{bmatrix}^\top,$$

where $\ell(j)$ denotes the assignment of landmark $\mathbf{m}^j$ to measurement $\mathbf{z}^{\ell(j)}$ and M the total number of associated landmarks.

B. Optimal Importance Density Approximation

The choice of importance density $q(\mathbf{s}_k^{(i)} | \mathbf{s}_{0:k-1}^{(i)}, \mathcal{Z}_{1:k}, \mathbf{u}_{1:k})$ in (9) is a crucial aspect of particle filtering which considerably affects the performance of the filter. In order to minimize the variance of weight increment in (9), new samples for $\mathbf{x}_k$ should be drawn according to the OID given by [17]

$$\begin{aligned} q(\mathbf{s}_k^{(i)} | \mathbf{s}_{0:k-1}^{(i)}, \mathcal{Z}_{1:k}, \mathbf{u}_{1:k}) &= p(\mathbf{x}_k^{(i)} | \mathbf{x}_{k-1}^{(i)}, \mathbf{y}_k, \mathbf{u}_k) \\ &\propto p(\mathbf{y}_k | \mathbf{x}_k^{(i)}) p(\mathbf{x}_k^{(i)} | \mathbf{x}_{k-1}^{(i)}, \mathbf{u}_k), \end{aligned} \tag{10}$$

where the superscript i is omitted for brevity in the following.

Since the motion and measurement models are nonlinear, the OID cannot be sampled from. One way to address this is to approximate (10) with a density that can be sampled from instead. Here, we use a Gaussian approximation of the form

$$p(\mathbf{x}_k | \mathbf{x}_{k-1}, \mathbf{y}_k, \mathbf{u}_k) \approx \mathcal{N}\left(\mathbf{x}_k; \boldsymbol{\mu}_k^{\mathbf{x}|\mathbf{y}}, \boldsymbol{\Sigma}_k^{\mathbf{x}|\mathbf{y}}\right). \tag{11}$$

This can be found by first finding the approximation

$$p(\mathbf{x}_k, \mathbf{y}_k | \mathbf{x}_{k-1}, \mathbf{u}_k) \approx \mathcal{N}\left(\begin{bmatrix} \mathbf{x}_k \\ \mathbf{y}_k \end{bmatrix}; \begin{bmatrix} \boldsymbol{\mu}_k^{\mathbf{x}} \\ \boldsymbol{\mu}_k^{\mathbf{y}} \end{bmatrix}, \begin{bmatrix} \boldsymbol{\Sigma}_k^{\mathbf{xx}} & \boldsymbol{\Sigma}_k^{\mathbf{xy}} \\ \boldsymbol{\Sigma}_k^{\mathbf{yx}} & \boldsymbol{\Sigma}_k^{\mathbf{yy}} \end{bmatrix}\right), \tag{12}$$

followed by conditioning on $\mathbf{y}_k$. This yields

$$\boldsymbol{\mu}_k^{\mathbf{x}|\mathbf{y}} = \boldsymbol{\mu}_k^{\mathbf{x}} + \boldsymbol{\Sigma}_k^{\mathbf{xy}} \left(\boldsymbol{\Sigma}_k^{\mathbf{yy}}\right)^{-1} \left(\mathbf{y}_k - \boldsymbol{\mu}_k^{\mathbf{y}}\right), \tag{13a}$$
$$\boldsymbol{\Sigma}_k^{\mathbf{x}|\mathbf{y}} = \boldsymbol{\Sigma}_k^{\mathbf{xx}} - \boldsymbol{\Sigma}_k^{\mathbf{xy}} \left(\boldsymbol{\Sigma}_k^{\mathbf{yy}}\right)^{-1} \boldsymbol{\Sigma}_k^{\mathbf{yx}}. \tag{13b}$$

Algorithm 2 IPL OID approximation

1: Set $\boldsymbol{\mu}_\pi^{\mathbf{x},0} = \mathrm{E}\{\mathbf{x}_n \mid \mathbf{x}_{n-1}^{(i)}\}$ and $\boldsymbol{\Sigma}_\pi^{x,0} = \mathrm{Cov}\{\mathbf{x}_n \mid \mathbf{x}_{n-1}^{(i)}\}$
2: **for** $l = 1, \dots, L$ **do**
3: Calculate $\boldsymbol{\mu}_\pi^{\mathbf{y},l}$, $\boldsymbol{\Sigma}_\pi^{\mathbf{y},l}$, and $\boldsymbol{\Sigma}_\pi^{\mathbf{xy},l}$ using (14) and $\boldsymbol{\mu}_\pi^{\mathbf{x},l-1}$, $\boldsymbol{\Sigma}_\pi^{\mathbf{x},l-1}$
4: Calculate $\mathbf{A}^l$, $\mathbf{b}^l$, and $\boldsymbol{\Omega}^l$ using (16)
5: Calculate $\boldsymbol{\mu}_k^{\mathbf{x}|\mathbf{y},l}$ and $\boldsymbol{\Sigma}_k^{\mathbf{x}|\mathbf{y},l}$ using (13) and (17)
6: Set $\boldsymbol{\mu}_\pi^{\mathbf{x},l} \leftarrow \boldsymbol{\mu}_k^{\mathbf{x}|\mathbf{y},l}$ and $\boldsymbol{\Sigma}_\pi^{\mathbf{x},l} \leftarrow \boldsymbol{\Sigma}_k^{\mathbf{x}|\mathbf{y},l}$
7: **end for**

C. Statistical Linear Regression and Posterior Linearization

The main problem in finding the approximation (12) is to determine the mean $\boldsymbol{\mu}_k^{\mathbf{y}}$ and covariance matrices $\boldsymbol{\Sigma}_k^{\mathbf{yy}}$ and $\boldsymbol{\Sigma}_k^{\mathbf{xy}}$. To this end, we use an approach based on generalized SLR and IPL [13], [14] as outlined below.

Let $\mathbf{x} \sim \pi(\mathbf{x})$ with mean $\boldsymbol{\mu}_\pi^{\mathbf{x}}$ and covariance $\boldsymbol{\Sigma}_\pi^{\mathbf{xx}}$, and $\mathbf{y} \sim p(\mathbf{y}|\mathbf{x})$ with conditional moments $\mathrm{E}\{\mathbf{y}|\mathbf{x}\}$ and $\mathrm{Cov}\{\mathbf{y}|\mathbf{x}\}$. Using conditional expectations, it follows that [19]

$$\boldsymbol{\mu}_\pi^{\mathbf{y}} = \mathrm{E}_\pi\left\{\mathrm{E}\{\mathbf{y}|\mathbf{x}\}\right\}, \tag{14a}$$
$$\boldsymbol{\Sigma}_\pi^{\mathbf{yy}} = \mathrm{Cov}_\pi\left\{\mathrm{E}\{\mathbf{y}|\mathbf{x}\}\right\} + \mathrm{E}_\pi\left\{\mathrm{Cov}\{\mathbf{y}|\mathbf{x}\}\right\}, \tag{14b}$$
$$\boldsymbol{\Sigma}_\pi^{\mathbf{yx}} = \mathrm{Cov}_\pi\left\{\mathrm{E}\{\mathbf{y}|\mathbf{x}\}, \mathbf{x}\right\}, \tag{14c}$$

where the expectations are with respect to $\pi(\mathbf{x})$ as denoted by the subscript π. Then, generalized SLR finds the affine approximation [13], [19]

$$\mathbf{y} \approx \mathbf{A}\mathbf{x} + \mathbf{b} + \mathbf{v}, \tag{15a}$$
$$\mathbf{v} \sim \mathcal{N}(\mathbf{0}, \boldsymbol{\Omega}), \tag{15b}$$

with respect to $\pi(\mathbf{x})$, where

$$\mathbf{A} = \boldsymbol{\Sigma}_\pi^{\mathbf{yx}} \left(\boldsymbol{\Sigma}_\pi^{\mathbf{xx}}\right)^{-1}, \tag{16a}$$
$$\mathbf{b} = \boldsymbol{\mu}_\pi^{\mathbf{y}} - \mathbf{A}\boldsymbol{\mu}_\pi^{\mathbf{x}}, \tag{16b}$$
$$\boldsymbol{\Omega} = \boldsymbol{\Sigma}_\pi^{\mathbf{yy}} - \mathbf{A}\boldsymbol{\Sigma}_\pi^{\mathbf{xx}}\mathbf{A}^\top. \tag{16c}$$

Given the linearization (15)–(16), the approximation of the OID with respect to the linearization density $\pi(\mathbf{x})$ then is

$$\boldsymbol{\mu}_k^{\mathbf{y}} = \mathbf{A}\boldsymbol{\mu}_k^{\mathbf{x}} + \mathbf{b}, \tag{17a}$$
$$\boldsymbol{\Sigma}_k^{\mathbf{y}} = \mathbf{A}\boldsymbol{\Sigma}_k^{\mathbf{xx}}\mathbf{A}^\top + \boldsymbol{\Omega}, \tag{17b}$$
$$\boldsymbol{\Sigma}_k^{\mathbf{xy}} = \boldsymbol{\Sigma}_k^{\mathbf{xx}}\mathbf{A}^\top. \tag{17c}$$

The choice of the linearization density $\pi(\mathbf{x})$ is key for approximating the OID well. Ideally, linearization is done with respect to the OID itself (posterior linearization). However, since this is unavailable to begin with, IPL [13] can be used.

IPL iteratively refines the OID approximation by first calculating an approximation based on the prior, in this case the dynamic model $p(\mathbf{x}_k|\mathbf{x}_{k-1}, \mathbf{u}_k)$. This first linearization is used to obtain a first approximation of the OID. Next, the approximation of the OID is used to find a better linearization, and then to find an improved OID approximation. This is repeated either for a fixed number of iterations or until the OID has converged [14] and is summarized in Algorithm 2. Note that Algorithm 2 is run for each particle individually, resulting in individual OID approximations for each particle.

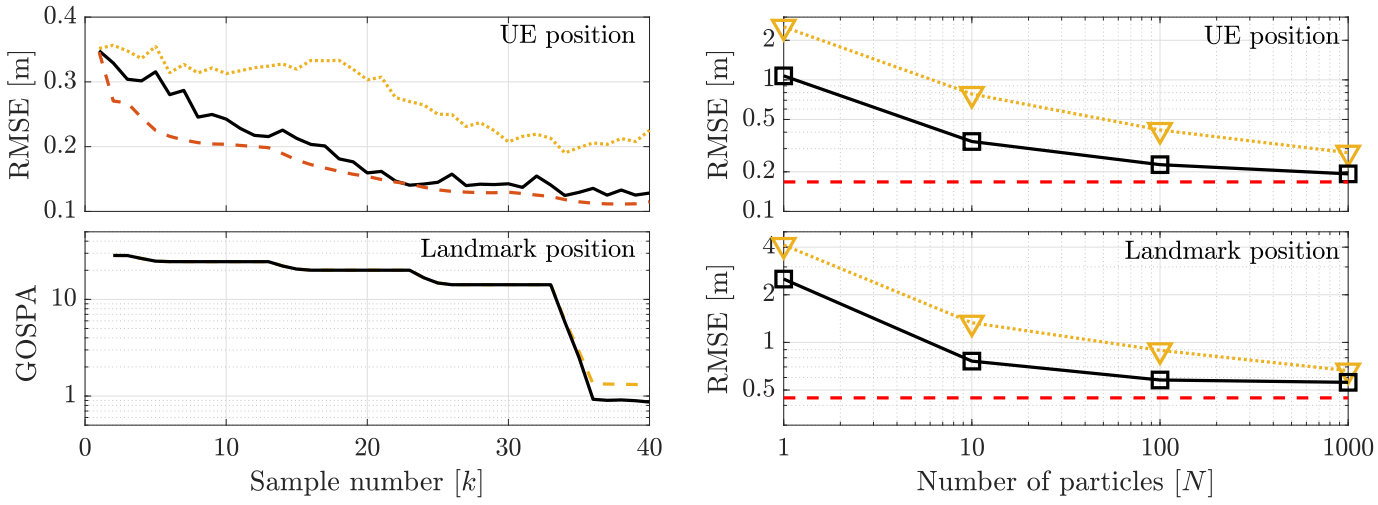

Fig. 2. In (a), RMS positioning error and GOSPA for each time step k and in (b), RMS positioning error of the UE and landmarks as a function of N. The PCRB illustrated using (- - -) and the PHD-SLAM filter using the motion model as the importance density (·····) and the proposed importance density (——).

IV. Numerical Evaluation

A. Simulation Setup

The UE motion is modeled using a coordinated turn model and a 360° turn is conducted around a BS. The landmark states are unknown and there are four VAs and four SPs in the surrounding environment. The VAs are always visible whereas the SPs are only visible if they are within the SP FOV. More details on the experimental setting can be found in [6] and the parameters are the same as used in [9]. The OID approximation uses, $L = 5$, iterations unless otherwise stated. In this paper, the PHD update step in (5) and the moments in (14) are computed using Taylor series based approximations.

The UE state is estimated using weighted sum of the particles [11] and the landmarks are estimated using the method described in [20, Table III]. State estimation accuracy is assessed using the root mean squared error (RMSE) and mapping performance with the generalized optimal subpattern assignment (GOSPA) metric [21]. The proposed filter is evaluated with respect to the posterior Cramér-Rao bound (PCRB) [9] and benchmarked against another PHD-SLAM filter that uses the motion model as the importance density [6]. Comparison to [12] will also be discussed at the end of the section. Overall, 100 Monte Carlo simulations are performed with every parameter setting and the results are obtained by averaging over the different simulations.

B. Results

The positioning accuracy of the UE and GOSPA for the landmarks are illustrated in Fig. 2(a) using $N = 1000$. As the UE cycles the BS, the positioning accuracy of the VAs improve as more measurements are received and as the geometric dilution of precision decreases. Moreover, the SPs are localized once in the FOV and as a result, the GOSPA gradually decreases. The notable steps in GOSPA correspond to time instances the SPs are within the FOV for the first time and miss detection is not penalized by the GOSPA metric anymore. As the map accuracy increases, also the root mean squared (RMS) positioning error of the UE decreases. As shown, the presented filter together with the iterative OID approximation nearly achieves the PCRB outperforming the filter that uses the motion model as the importance density. The RMSEs of the other states are summarized in Table I.

The positioning accuracy of the UE and landmarks as a function of number of particles are illustrated in Fig. 2(b). As shown, using the iterative OID approximation, the number of required particles is approximately 40 times lower than with the benchmark solution. The main reason for this difference is that using the motion model as the importance density leads to an inefficient sample approximation as most of the particles are located where the posterior is close to zero. More quantitatively, the relative effective sample size (ESS) is 48.3% using the proposed importance density and 2.4% using the motion model. Thus, the benchmark filter requires far more particles to approximate the UE posterior accurately.

Performance of the proposed method for different number of iterations L is summarized in Table I. In general, the accuracy of PHD-SLAM improves as L grows and since the result does not improve after three iterations, results for $L > 3$ are not shown. In the table, results for different number of particles are also shown for which N is selected so that the computation time is equal to 500 ms which corresponds to the sampling interval. As tabulated in Table I, the added computational complexity for $L > 0$ can be easily justified by the more efficient use of particles which results to superior performance. If only a fraction of the computational resources can be reserved for Radio-SLAM, good accuracy and real-time operation can still be accomplished using $L > 0$. As an example, comparative

TABLE I
PERFORMANCE OF PHD-SLAM FOR DIFFERENT NUMBER OF OID APPROXIMATION ITERATIONS L AND PARTICLES N.

		UE / Vehicle			Landmark		Average / iteration	
L	N	Position [m]	Heading [deg]	Clock bias [ns]	Position [m]	GOSPA	ESS [%]	Time [ms]
0	1000	0.279	0.192	0.433	0.663	1.310	2.416	756
1	1000	0.195	0.140	0.341	0.562	0.880	48.115	1125
2	1000	0.193	0.137	0.338	0.560	0.868	48.235	1312
3	1000	0.193	0.137	0.338	0.559	0.867	48.252	1321
0	661	0.337	0.227	0.482	0.754	1.628	2.517	500
1	444	0.204	0.143	0.353	0.564	0.953	49.233	500
5	379	0.204	0.140	0.341	0.563	0.870	49.436	500
5	25	0.288	0.173	0.461	0.667	1.308	56.280	33

performance to $N = 1000$ and $L = 0$ can be achieved with only 25 particles and using $L = 5$.

There is a direct relationship of the proposed OID approximation to importance densities used in earlier SLAM works. Selecting $L = 0$, lines $2-7$ of Algorithm 2 are not computed and the OID approximation is equivalent to the importance density used in [6], [7]. On the other hand, selecting $L = 1$, linearization is performed around the prior mean and the proposed method is equivalent to the one-step OID approximation used in FastSLAM 2.0 [12]. It is worth noting that previous works in Radio-SLAM have only used the motion model as the importance density and as we have shown, the one-step and iterative OID approximations yield outstanding performance and their use is highly recommended. In future research, we will explore more complex and realistic experimental settings and investigate whether the proposed method bring further advantages over the one-step OID approximation used in FastSLAM 2.0.

V. CONCLUSIONS

In this paper, we have provided the details to iteratively approximate the optimal importance density and utilized the method in a probability hypothesis density (PHD) simultaneous localization and mapping (SLAM) filter. The proposed method is demonstrated in a 5G downlink scenario and the simulation results imply a significant increase in the average effective sample size. This improvement enables the proposed system to achieve comparative performance and a reduced computational overhead, or superior accuracy and a comparative run-time with respect to a benchmark PHD-SLAM solution. The development efforts of this paper take performing high accuracy and real-time Radio-SLAM in future 5G and beyond networks one step closer.

REFERENCES

[1] C. De Lima *et al.*, "Convergent communication, sensing and localization in 6G systems: An overview of technologies, opportunities and challenges," *IEEE Access*, vol. 9, pp. 26 902–26 925, 2021.

[2] A. Shahmansoori, G. E. Garcia, G. Destino, G. Seco-Granados, and H. Wymeersch, "Position and orientation estimation through millimeter-wave MIMO in 5G systems," *IEEE Transactions on Wireless Communications*, vol. 17, no. 3, pp. 1822–1835, 2018.

[3] H. Wymeersch, G. Seco-Granados, G. Destino, D. Dardari, and F. Tufvesson, "5G mmWave positioning for vehicular networks," *IEEE Wireless Communications*, vol. 24, no. 6, pp. 80–86, 2017.

[4] A. Yassin, Y. Nasser, A. Y. Al-Dubai, and M. Awad, "MOSAIC: Simultaneous localization and environment mapping using mmWave without a-priori knowledge," *IEEE Access*, vol. 6, pp. 68 932–68 947, 2018.

[5] E. Leitinger, F. Meyer, F. Hlawatsch, K. Witrisal, F. Tufvesson, and M. Z. Win, "A belief propagation algorithm for multipath-based SLAM," *IEEE Transactions on Wireless Communications*, vol. 18, no. 12, pp. 5613–5629, 2019.

[6] H. Kim, K. Granström, L. Gao, G. Battistelli, S. Kim, and H. Wymeersch, "5G mmWave cooperative positioning and mapping using multi-model PHD filter and map fusion," *IEEE Transactions on Wireless Communications*, vol. 19, no. 6, pp. 3782–3795, 2020.

[7] Y. Ge, F. Wen, H. Kim, M. Zhu, F. Jiang, S. Kim, L. Svensson, and H. Wymeersch, "5G SLAM using the clustering and assignment approach with diffuse multipath," *Sensors*, vol. 20, no. 16, 2020.

[8] Y. Ge, O. Kaltiokallio, H. Kim, F. Jiang, J. Talvitie, M. Valkama, L. Svensson, S. Kim, and H. Wymeersch, "A computationally efficient EK-PMBM filter for bistatic mmWave radio SLAM," *IEEE Journal on Selected Areas in Communications*, early access, Mar. 2, 2022.

[9] O. Kaltiokallio, Y. Ge, J. Talvitie, H. Wymeersch, and M. Valkama, "mmWave simultaneous localization and mapping using a computationally efficient EK-PHD filter," in *FUSION*, 2021.

[10] Y. Ge, Y. Wu, F. Jiang, O. Kaltiokallio, J. Talvitie, M. Valkama, L. Svensson, and H. Wymeersch, "Iterated posterior linearization PMB filter for 5G SLAM," in *ICC 2022*, to be published.

[11] J. Mullane, B.-N. Vo, M. D. Adams, and B.-T. Vo, "A random-finite-set approach to Bayesian SLAM," *IEEE Transactions on Robotics*, vol. 27, no. 2, pp. 268–282, 2011.

[12] M. Montemerlo, S. Thrun, D. Roller, and B. Wegbreit, "FastSLAM 2.0: An improved particle filtering algorithm for simultaneous localization and mapping that provably converges," in *IJCAI*, 2003.

[13] Á. F. García-Fernández, L. Svensson, M. R. Morelande, and S. Särkkä, "Posterior linearization filter: Principles and implementation using sigma points," *IEEE Transactions on Signal Processing*, vol. 63, no. 20, pp. 5561–5573, October 2015.

[14] R. Hostettler, F. Tronarp, Á. F. García-Fernández, and S. Särkkä, "Importance densities for particle filtering using iterated conditional expectations," *IEEE Signal Processing Letters*, vol. 27, no. 1, pp. 211–215, December 2020.

[15] B.-N. Vo and W.-K. Ma, "The Gaussian mixture probability hypothesis density filter," *IEEE Transactions on Signal Processing*, vol. 54, no. 11, pp. 4091–4104, 2006.

[16] Y. Bar-Shalom, T. Kirubarajan, and X.-R. Li, *Estimation with Applications to Tracking and Navigation*. John Wiley & Sons, Inc., 2002.

[17] A. Doucet and A. M. Johansen, "A tutorial on particle filtering and smoothing: Fifteen years later," in *Handbook of Nonlinear Filtering*, ser. Oxford Handbooks, D. Crisan and B. Rozovskii, Eds. Oxford, UK: Oxford University Press, 2011, vol. 12, pp. 656–704.

[18] S. S. Blackman and R. Popoli, *Design and analysis of modern tracking systems*. Artech House, 1999.

[19] F. Tronarp, Á. F. García-Fernández, and S. Särkkä, "Iterative filtering and smoothing in nonlinear and non-Gaussian systems using conditional moments," *IEEE Signal Processing Letters*, vol. 25, no. 3, pp. 408–412, March 2018.

[20] B.-N. Vo, B.-T. Vo, and D. Phung, "Labeled random finite sets and the Bayes multi-target tracking filter," *IEEE Transactions on Signal Processing*, vol. 62, no. 24, pp. 6554–6567, 2014.

[21] A. S. Rahmathullah, A. F. García-Fernández, and L. Svensson, "Generalized optimal sub-pattern assignment metric," in *FUSION*, 2017.